

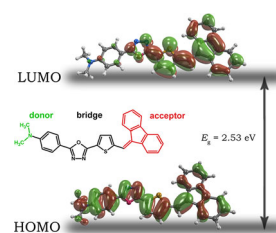
Theoretical and experimental study of donor-bridge-acceptor system: model 2-[5-(9*H*-fluoren-9-ylidenemethyl)thiophen-2-yl]-1,3,4-oxadiazole derivatives

Martin Michalík¹ · Anita Andicsová Eckstein² · Erika Kozma³ · Francesco Galeotti³ · Vladimír Lukeš¹ · Pavel Hrdlovič² · Daniel Végh⁴

Received: 2 June 2016 / Accepted: 1 September 2016
© Springer-Verlag Wien 2016

Abstract The theoretical study of the titled model acceptor-bridge-donor molecular series based on 9*H*-fluoren-9-ylidenemethyl and 1,3,4-oxadiazole heterocycles is presented. The subunits are linked through a thienyl moiety, and the second α -site of oxadiazole was modified. The quantum chemical model indicated that the electron-donating properties of 9*H*-fluoren-9-ylidenemethyl were significantly supported or suppressed by the terminal substitution of 1,3,4-oxadiazole which affected the possible semiconductivity. Finally, the possible synthesis of selected molecules is described, and the prepared derivatives were fully characterized by ¹H NMR, ¹³C NMR, IR, and elemental analysis together with optical and electrochemical measurements.

Graphical abstract



Keywords Heterocycles · Absorption spectra · Electronic structure · Computational chemistry

Introduction

Conjugated organic molecules with suitable physical-chemical properties are attractive modern materials for academic and industrial applications. The small molecular units in comparison with their polymer counterparts have the advantage of a better synthetic reproducibility, higher purity, and no batch-to-batch modification. In the last years, organic molecule-based materials became a key factor in the development of many fields, such as organic solar cells [1–3], electroluminescent devices [4], memory devices, sensors, transistors, batteries, photoreceptors, and displays [5]. Very often, the modern material research of novel organic molecules suitable for the application in electronics is connected with the tuning of the optical and electrochemical properties, e.g., using the combination of chromophoric moieties. Synthetic strategies for the optimization of material properties could involve the addition of an electron donor (D) and/or acceptor (A) substituents in the specific positions

Electronic supplementary material The online version of this article (doi:10.1007/s00706-016-1843-2) contains supplementary material, which is available to authorized users.

✉ Martin Michalík
martin.michalik@stuba.sk

¹ Department of Chemical Physics, Slovak University of Technology, Radlinského 9, SK-812 37 Bratislava, Slovak Republic

² Polymer Institute, Slovak Academy of Sciences, Dúbravská Cesta 9, 845 41 Bratislava, Slovak Republic

³ Istituto per lo Studio delle Macromolecole, Consiglio Nazionale delle Ricerche, Via Corti 12, 20133 Milan, Italy

⁴ Department of Organic Chemistry, Slovak University of Technology, Radlinského 9, SK-812 37 Bratislava, Slovak Republic

of the molecule which modulate the energy gaps between the frontier molecular orbitals, i.e., highest occupied (HOMO) and lowest unoccupied (LUMO) molecular orbitals. Energy gap between the HOMO and the LUMO is closely related to the solid-state bandgap, although the latter is usually lower. From the macroscopic point of view, the electric semiconductivity in the organic materials is also dependent on the position of Fermi energy level and the energy bandgap between the valence and conduction bands. In general, electric conductivity increases with the reduction of the energy bandgap [6].

Fluorene and thiophene derivatives [7, 8] usually form the representative components in several oligomers or polymers for the construction of light-emitting materials [9]. Among these molecules, the fluorene units are often added through single bonds at 2,7 sites [10]. The alkyl chains connected to the C9 fluorene atom improves the solubility and the incorporation into the polymer matrix. Besides, the presence of 1,3,4-oxadiazole units can support the charge-transport properties as well as the thermal stability [11]. In addition, the oxadiazole compounds possess a broad biological activity [12] and are utilized in many pharmaceuticals [13, 14] and agrochemicals [15]. From the chemical point of view, the 1,3,4-oxadiazole linked through a thienyl moiety to the 9*H*-fluorene-9-ylidene-methyl unit represents the unique combination which was not investigated and published in the literature yet. With thienyl group as linker between these chromophoric pair conjugation, length is extended what could play an important role in electronic devices [16]. It is plausible to suppose that the terminal substitution of 1,3,4-oxadiazole is able to modify the electron structure and electron-donating properties of 9*H*-fluorene-9-ylidene-methyl unit. These modifications using the end-capping group method are now frequently used in a novel material development [17, 18].

Herein, we report the theoretical and subsequent experimental study of novel representative derivatives of 2-[5-(9*H*-fluorene-9-ylidene-methyl)thiophen-2-yl]-1,3,4-oxadiazole. The chemical structures of the acceptor-bridge-donor

systems and their notation are presented in Fig. 1. The partial aims of this study are: (1) to investigate systematically the role of substitution on the electronic structure using the density functional theory; (2) to suggest the possible synthetic route; and (3) to apply it for the synthesis of selected molecules. Finally, the theoretical data will be compared with the absorption spectra and electrochemical measurements of synthesized molecules. Based on the molecular orbital analysis, we will specify which studied derivatives with minimal corresponding energy gap prefer p-type (low-lying HOMO) or n-type semiconductivities (high-lying LUMO).

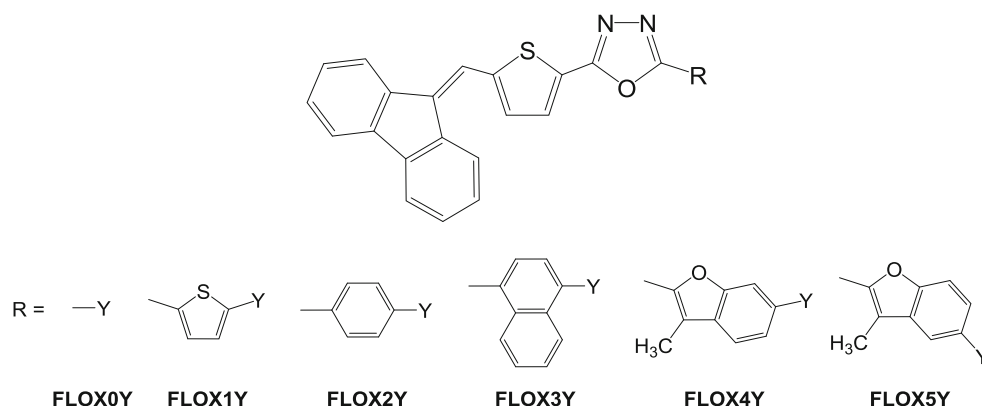
Results and discussion

Theoretical geometries and electronic structure

Aromatic rings of the studied compounds are connected by single bonds which lead to numerous possible conformations with respect to the spatial setting. In the case of three five-membered heterocyclic unit connection, up to four conformations can be considered. As it is presented for parental compounds ($Y = H$) in Table 1S and Fig. 1S, all-anti conformations are slightly energetically favored for **FLOX0c** and **FLOX1c**. At the B3LYP/6-31+G(d,p) level of the theory, the minimal Gibbs free-energy difference of 2.5 kJ mol^{-1} between all-anti and all-syn conformations at 298 K is found for **FLOX1c**. The minimal steric repulsion and the global minima on the potential energy surface were also theoretically predicted for unsubstituted all-anti oligothiophenes [19]. On the other hand, the presence of methyl group at the alpha site of benzofuran prefers the anti-syn conformation by 10.7 kJ mol^{-1} . The B3LYP calculation for the benzofuran derivative without the methyl group revealed the lower energy difference of 3.1 kJ mol^{-1} . In the case of **FLOX2c** and **FLOX3c**, the energetically favored conformation depicted in Fig. 1Sa will be denoted as all-anti.

Due to the large variability of possible orientations of dihedral angles between the aromatic rings, in the

Fig. 1 Chemical structure and notation of studied **FLOX** molecules according to the added $-R$ group. The substituents $-Y$ are **a** $-\text{N}(\text{CH}_3)_2$, **b** $-\text{NH}_2$, **c** $-\text{H}$, **d** $-\text{CF}_3$, and **e** $-\text{NO}_2$



preliminary screening, all-anti orientation of side chain rings was selected for latter 23 derivatives ($Y \neq H$).

The top views on the optimized gas-phase B3LYP all-anti geometries of selected **FLOX** molecules are presented in Fig. 2S. These geometries are practically planar. The maximal distortion of 10° was indicated between the thiophene plane and the ylidene carbon atoms. Only in the case of **FLOX3Y** molecules, the mutual orientation of naphthyl moieties and 1,3,4-oxadiazole was 30° .

The gas-phase B3LYP energies of frontier orbitals and the corresponding energy gaps for **FLOX** series in all-anti conformations are presented in Table 1 which also show the influence of ring termination and -Y substituent on the HOMO and LUMO energies. For example, the higher HOMO energy exhibits the compounds containing strong electron-donating -N(CH₃)₂ or -NH₂ groups. On the other hand, the presence of

the strong electron-withdrawing nitro group decreases the HOMO energy by about 0.45 eV with respect to the parental compounds end-capped with hydrogen atom, i.e., $Y = H$.

The substituent effect can also be expressed by the correlation of HOMO energies on the Hammett substituent constants. The published values for para substituent effect are -0.83 for -N(CH₃)₂, -0.66 for -NH₂, 0.00 for -H, 0.54 for -CF₃, and 0.78 for NO₂ [20]. The data presented in Fig. 3S show the linear properties for all five molecular series. All regression coefficients are better than 0.96. The minimal substituent effect was found for the **FLOX5** derivatives having the slope of -0.28 eV. The highest sensitivity to the substituent change exhibits the **FLOX0** series which has the shortest π -conjunction length. The corresponding slope is -0.50 eV. The slopes of the rest molecular series range from -0.43 to -0.34 eV.

Table 1 Theoretical gas-phase B3LYP/6-31+G(d,p) HOMO (E_{HOMO}) and LUMO (E_{LUMO}) energies, energy gaps ($E_{\text{gap}} = E_{\text{LUMO}} - E_{\text{HOMO}}$), and electric dipole moments (μ) of studied molecules in all-anti conformation

Derivative	$E_{\text{HOMO}}/\text{eV}$	$E_{\text{LUMO}}/\text{eV}$	E_{gap}/eV	μ/D
FLOX0a	-5.50	-2.54	2.97	5.23
FLOX0b	-5.65	-2.61	3.04	4.61
FLOX0c	-5.90	-2.79	3.10	3.88
FLOX0d	-6.20	-2.98	3.22	5.69
FLOX0e	-6.35	-3.66	2.70	8.18
FLOX1a	-5.30	-2.57	2.73	6.72
FLOX1b	-5.47	-2.63	2.84	5.90
FLOX1c	-5.75	-2.78	2.98	4.40
FLOX1d	-5.93	-2.98	2.95	5.86
FLOX1e	-6.05	-3.54	2.51	8.30
FLOX2a	-5.40	-2.57	2.83	7.03
FLOX2b	-5.55	-2.62	2.93	5.91
FLOX2c	-5.77	-2.76	3.02	3.90
FLOX2d	-5.92	-2.94	2.99	4.19
FLOX2e	-6.01	-3.35	2.66	6.31
FLOX3a	-5.54	-2.66	2.88	5.06
FLOX3b	-5.48	-2.63	2.86	5.40
FLOX3c	-5.74	-2.75	2.99	4.07
FLOX3d	-5.90	-2.92	2.98	4.78
FLOX3e	-6.07	-3.27	2.80	7.05
FLOX4a	-5.26	-2.66	2.60	6.13
FLOX4b	-5.46	-2.69	2.77	5.62
FLOX4c	-5.74	-2.75	2.99	5.00
FLOX4d	-5.90	-2.94	2.95	7.12
FLOX4e	-5.98	-3.19	2.79	9.43
FLOX5a	-5.43	-2.72	2.71	6.62
FLOX5b	-5.64	-2.75	2.90	5.96
FLOX5c	-5.75	-2.80	2.95	5.00
FLOX5d	-5.89	-2.93	2.96	4.74
FLOX5e	-5.96	-3.04	2.92	6.03

Interestingly, the addition of $-\text{CF}_3$ and $-\text{NO}_2$ groups is able to shift LUMO energies under -3.3 eV. The introduction of the substituent to the ring also modulates the energy gap. For example, the lowest energy gap of 2.51 eV is predicted for the nitrothiophene containing **FLOX1e** molecule. As it is indicated in Table 1, the energy gaps of compounds containing electron-donating dimethylamino group are changed from 2.60 to 2.97 eV. Contrary to the HOMO energies, worse linear correlation of LUMO energies with Hammett constants was found (see Fig. 4S). The regression coefficients range from 0.89 to 0.96.

The influence of the terminal electron-donating and electron-withdrawing substitutions of end-capped aromatic rings on the electronic structure can be estimated from the electron density distribution or the shape of frontier molecular orbitals. As it is presented in Fig. 2 for the **FLOX2a** and **FLOX2b** molecules, the HOMO orbitals are not dominantly delocalized over 9*H*-fluoren-9-ylidene-methyl unit.

On the other hand, the presence of strong electron-withdrawing groups $-\text{CF}_3$ and $-\text{NO}_2$ supports the uniform delocalization of HOMO electron over the 9*H*-fluoren-9-

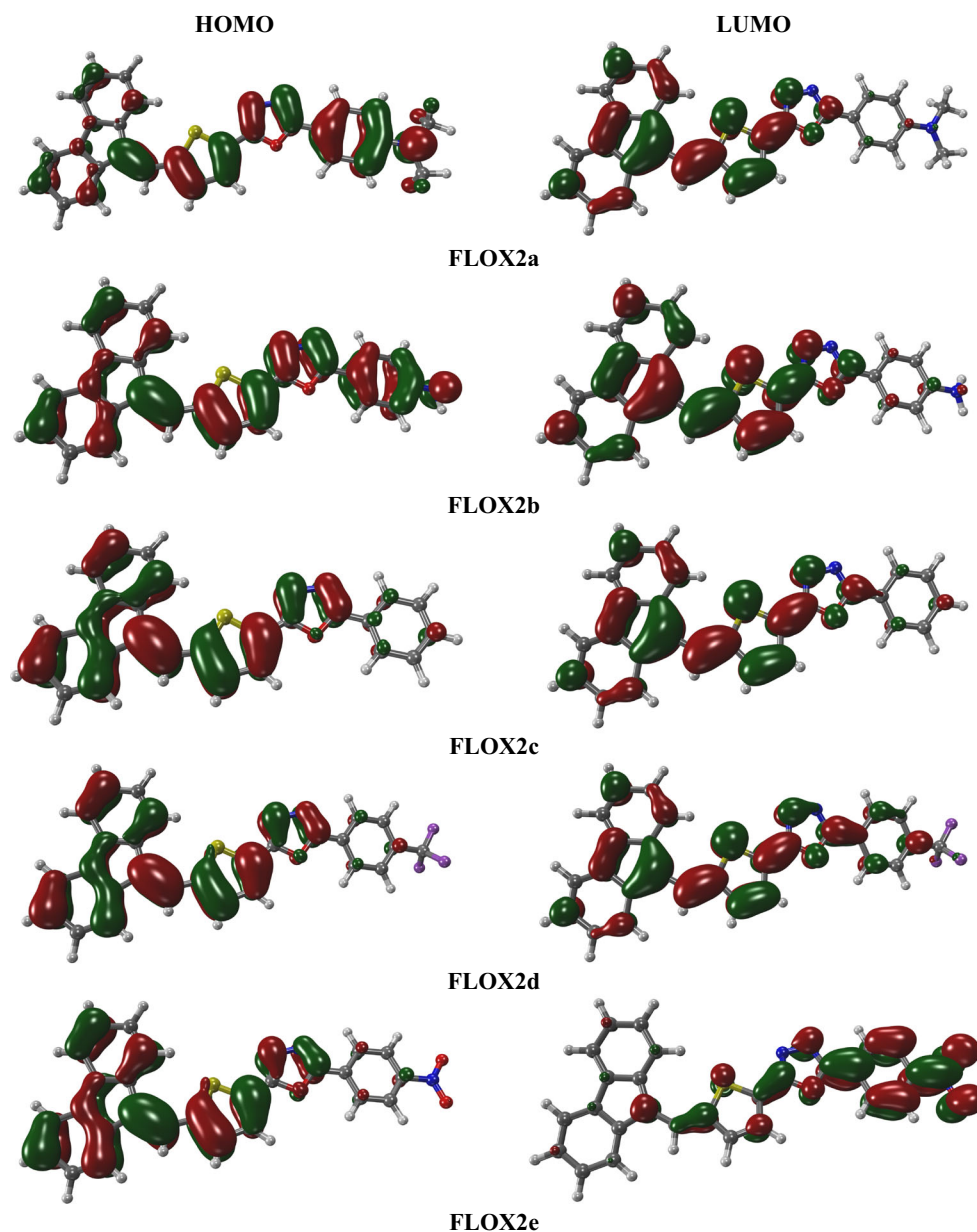


Fig. 2 Influence of Y substitution on the *shape* of the B3LYP/6-31+G(d,p) frontier molecular orbitals for **FLOX2Y** molecules in all-anti conformations (isovalue = $0.02 \text{ bohr}^{-3/2}$)

ylidenemethyl unit, thienyl C–C bonds neighbouring the sulfur atom and C–N bonds of oxadiazole.

In the case of LUMOs, the substitution has the opposite role (see also Fig. 5S for other derivatives). It seems that the electron-donating properties of 9H-fluoren-9-ylidenemethyl unit are significantly supported or suppressed by the terminal Y group. Although the electric conductivity is affected by the mutual orientation of neighboring molecule, the electron charge distribution over one molecule is also important. The p-type semiconductivity is connected with the positive charge transport which prefers the molecular parts with the excess of π -electron charge density. In addition, the n-type semiconductivity is based on the negative charge shifting along the electron-deficient parts.

As it was mentioned by Blouin et al. [21], the ideal HOMO energy level should range between -5.2 and -5.8 eV, while as for ideal donor, LUMO energy should be in the range -3.7 and -4.0 eV. With respect to our predictions, the investigated molecular series could potentially satisfy p-type semiconductivity criterion.

Finally, the presence of substituent has the direct influence on the electric microscopic properties. The calculated gas-phase electric dipole moments for all-anti unsubstituted molecules reached the minimal values from 3.88 to 5.00 D. The maximal values of 6.03 to 9.43 D are observed mostly for NO_2 substitution. In the case of diphenylamine substituent, the values are from 5.06 to 7.03 D. Interestingly, the dependence of evaluated dipole moments on the Hammett substituent constant has the parabolic shape (see Fig. 6S). As Table 2S illustrates for **FLOXYc** molecules, all-syn conformations show minimal dipole moments. Therefore, the Boltzmann weighted dipole moments are lower than all-anti ones.

Synthesis and experimental characterization of selected molecules

The following experimental part presents the possible synthetic route, as illustrated in the Scheme 1. These multi-step reactions with relatively high yields were used for preparation for all parental derivatives except for **FLOX0c**. With respect to the theoretical predictions and the reagents' availability, **FLOX2a** was also prepared.

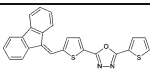
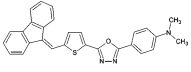
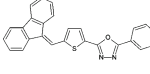
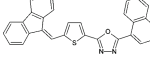
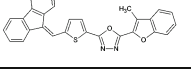
As a general synthetic procedure, the thiophene ring is connected with the fluorene chromophore through the double bonded carbon atom in a phase transfer reaction, using aqueous NaOH and toluene as a solvent, yielding the fluorenyl-thiophene derivative **1**. The formyl derivate **2** was prepared by means of Vilsmeier–Haack formulation (POCl_3/DMF) in 91% yield. Compound **3** was obtained in 80% yield and then treated with $\text{NaN}_3/\text{Et}_3\text{N}\cdot\text{HCl}$ in toluene at 180°C affording the tetrazole derivative **4** in 92% yield. Finally, the last step of the synthetic procedure yields the asymmetrically

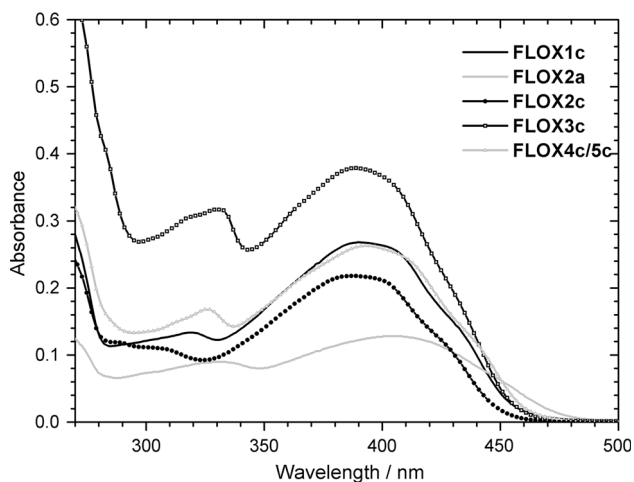
disubstituted-1,3,4-oxadiazoles, by the Huisgen reaction of compound **4** with the corresponding acyl chloride. The purification of the crude products by silica gel column chromatography using hexane/ethylacetate (9/1) mixture as eluent gives **FLOX** derivatives in 52–72% yields (Table 2). The comparison of melting point shows that the highest thermal stability supports the connection of 1,3,4-oxadiazole with 3-methylbenzofuran-2-yl. From synthetic reasons, the methyl group is present in β -site of benzofuran in the case of **FLOX4** and **FLOX5** derivatives.

The experimental UV–Vis absorption spectra of studied molecules in dichloromethane solution are depicted in Fig. 3, showing the maximum absorption wavelengths (λ_{max}) ranging from 390 to 404 nm.

In general, all compounds have similar absorption features characterized by two broad main bands. The first intensive band occurs between 350 and 470 nm, and the second, less intensive absorption band is observed in the range of 280–350 nm. The TD-CAM-B3LYP//B3LYP/6-31+G(d,p) calculation for the gas phase showed that the lowest energy experimental band belongs to the electronic $S_0 \rightarrow S_1$ transition. This transition has a predominant $\pi - \pi^*$ character which is mostly connected with the electron excitation from HOMO to LUMO, as it demonstrated for **FLOX2a** and **FLOX2c** in Figs. 7S and 8S. All theoretical optical transition energies for **FLOX** molecules in all-anti conformation are collected in Table 3S. Substitution effect on the $S_0 \rightarrow S_1$ transition energies is predicted to be minimal, and this transition has the strongest oscillator strength compared to the first ten calculated ones. For example, the energies for **FLOX2Y** molecules are between 3.06 and 3.12 eV (405 and 398 nm). Furthermore, theoretical vertical optical transitions $S_0 \rightarrow S_2$ and $S_0 \rightarrow S_3$ shown in Fig. 9S with weak oscillator strength probably form the second experimental band. The molecular orbital analysis for **FLOX2a** and **FLOX2c** indicates that these transitions are connected with the HOMO–1 and HOMO–2 (Figs. 7S and 8S). Interestingly, the shapes of HOMO–2 for **FLOX2a** and HOMO–1 for **FLOX2c** are comparable, i.e., the lobes are delocalized over the fluorene unit. The experimental absorption spectra measured in methanol exhibit a very small solvent effect, and the uniform blueshift is ca. 3 nm. Moreover, the investigated molecules exhibit insignificant fluorescence. As shown in Table 4S, similar shifts are also predicted by theoretical calculations, including the solvent effect for methanol, dichloromethane, and water. The mutual comparison of Boltzmann weighted transition energies shows that the influence of solvent with respect to the gas phase is ca. 20 nm. Next, the electrochemical properties of prepared **FLOX** molecules were investigated to estimate frontier orbital energies. The dependences of oxidation potentials E_{ox}^0 vs standard calomel electrode (SCE) obtained from the

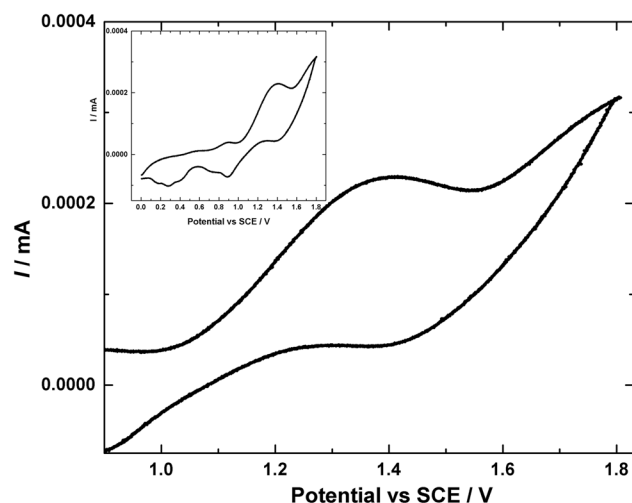
Table 2 Yields and melting points of selected **FLOXs**

Entry	Product	Yield / %	m.p. / °C
FLOX1c		60	177-180
FLOX2a		52	150-152
FLOX2c		63	168-169
FLOX3c		72	186-188
FLOX4c/5c		70	228-230

**Fig. 3** UV-Vis absorption spectra of prepared **FLOX** molecules in dichloromethane solution at 10^{-5} mol dm^{-3}

Conclusion

In this paper, the systematic quantum chemical study of novel electron acceptor-bridge-donor systems derived from the 2-[5-(9H-fluoren-9-ylidene-methyl)thiophen-2-yl]-1,3,4-oxadiazole was presented. On the selected molecules, we tried to theoretically demonstrate a way of energy-gap setting and possible activation of relevant molecule part which may play role in the electric semiconductivity or optical processes. The calculations indicated that the electron-donating properties of 9H-fluoren-9-ylidene-methyl unit are significantly supported by the electron-withdrawing Y groups or suppressed by the Y substitution at the side of 1,3,4-oxadiazole. Next, the Hammett-type dependencies were illustrated for the HOMO, LUMO

**Fig. 4** Cyclic voltammetry of **FLOX2a** measured in dichloromethane solution. Inset displays the broader potential window

energies, and dipole moments. Finally, the quantum chemical model predicted the derivatives with $-\text{N}(\text{CH}_3)_2$ as one of the most promising organic material with p-type semiconductivity.

Furthermore, the route for relatively high-yield synthesis was suggested, and five selected **FLOX** molecules were synthesized and chemically analyzed. The highest melting point exhibits the molecule containing 3-methylbenzofuran-2-yl, while the presence of phenyl group results in the lowest melting points. Experimental electrochemical and spectroscopic data supported the relevance of the used quantum chemical models. Results of our work can be further used for the synthesis of a broad range of small conjugated molecules with controlled electron acceptor-bridge-donor effect.

Experiment

All starting materials and substrates are commercially available (Sigma-Aldrich) and were used without further purification. Melting points were recorded on an electrothermal-9100 apparatus. All products were characterized by spectral data, including ^1H NMR, ^{13}C NMR, and FT-IR spectroscopy. The NMR spectra were obtained using VARIAN VXR 300 spectrometer. The infrared spectra (KBr) were determined on a Perkin-Elmer 1600 FT-IR system. The elemental analyses were performed by means of Carlo Erba Elemental Analyzer 1108. Silica gel 60 (230–400 mesh, Merck) was used for column chromatography. Reactions and the collected fraction samples were monitored by TLC (Merck 60 F254 silica gel). Visualization was made with UV light.

Table 3 Electrochemical characteristics and experimentally determined energies of frontier molecular orbitals for **FLOXs**

Sample	$E_{\text{ox}}^{1/2}/\text{V}$	$E_{\text{ox}}^{\text{p}}/\text{V}$	$E_{\text{HOMO}}(\text{exp})/\text{eV}$	$E_{\text{LUMO}}(\text{exp})/\text{eV}$	$E_{\text{g}}^{\text{opt}}/\text{eV}$
FLOX1c	1.51	1.64	-5.67	-3.08	2.64
FLOX2c	1.47	1.60	-5.63	-3.00	2.72
FLOX2a	1.18	1.41	-5.34	-2.87	2.53
FLOX3c	1.43	1.52	-5.59	-3.01	2.64
FLOX4c	1.47	1.57	-5.63	-3.00	2.76

$E_{\text{ox}}^{1/2}$ —halfway oxidation potential—and E_{ox}^{p} —peak reduction potential—were determined by cyclic voltammetry in 0.1 M TBAPF₆ in CH₂Cl₂ vs SCE, $E_{\text{g}}^{\text{opt}}$ experimental optical energy gap

2-(9H-Fluoren-9-ylidenemethyl)thiophene (**1**)

To the solution of 10.0 g fluorene (0.06 mol) and 6.7 g thiophene-2-carbaldehyde (0.06 mol) in 84 cm³ toluene, an aqueous solution of NaOH (56 g/84 cm³ water) and 3.5 g *n*-tetrabutylammonium bromide (0.01 mol) were added. The resulting heterogeneous mixture was vigorously stirred at room temperature for 3 h. After the reaction, the water layer was separated, and the organic layer was washed with 20 cm³ HCl (10%), 20 cm³ water, 30 cm³ brine, and dried over anhydrous Na₂SO₄. The isolated crude product was recrystallized from ethanol which afforded 8.1 g (85%) **1**. Yellow crystals; m.p.: 71–72 °C ([8] 72 °C); NMR, and IR spectra were found to be identical with the ones described in [8].

5-(9H-Fluoren-9-ylidenemethyl)thiophene-2-carbaldehyde (**2**, C₁₉H₁₂OS)

Phosphorus oxychloride (6.7 g, 44 mmol) was added dropwise under an argon atmosphere to 3.2 g *N,N*-dimethylformamide (44 mmol) at 5 °C. The solution was stirred for 30 min at room temperature. Subsequently, 3.5 g of **1** (22 mmol) in 5 cm³ *N,N*-dimethylformamide was added at room temperature. The reaction mixture was stirred at 80 °C for 3 h. The solution was poured to 50 cm³ of ice water and stirred with sodium carbonate to pH 7. The solution was filtered and washed by water. The crude product was recrystallized (ethanol), and we isolated the product **2** in 5.7 g (91%) yield. Yellow crystals; m.p.: 114 °C ([23] 113–115 °C); UV–Vis (dichloromethane, $c = 1 \times 10^{-5}$ mol dm⁻³): $\lambda_{\text{max}} = 238, 261, 366$ nm.

5-(9H-Fluoren-9-ylidenemethyl)thiophene-2-carbonitrile (**3**, C₁₉H₁₁NS)

A solution of 1 g carbaldehyde **2** (3.5 mmol) and 0.29 g NH₂OH•HCl (4.2 mmol) in 5.5 cm³ *N*-methyl-2-pyrrolidone was heated at 110–115 °C. After 8 h, the mixture was poured into 200 cm³ water and extracted with EtOAc (2 × 50 cm³). The combined organic layer was dried (Na₂SO₄), and the solvent was evaporated in vacuo. The separation of crude product by column chromatography (toluene) afforded 0.8 g (80%) **3**. Yellow crystals; m.p.:

163–164 °C; ¹H NMR (300 MHz, DMSO-*d*₆): $\delta = 7.25$ (t, 1H, $J = 1.12$ Hz, 7.82 Hz), 7.35 (t, 1H, $J = 1.25$ Hz, 7.44 Hz), 7.42 (t, 2H, $J = 0.96$ Hz, 7.45 Hz), 7.62 (d, 1H, $J = 3.92$ Hz), 7.83–7.89 (m, 4H), 7.96 (d, 1H, $J = 7.41$ Hz), 8.06 (d, 1H, $J = 3.92$ Hz) ppm; ¹³C NMR (75 MHz, DMSO-*d*₆): $\delta = 108.9, 114.1$ (CN), 117.4, 119.9, 120.4, 121.2, 124.1, 127.3, 127.4, 129.2, 129.7, 130.1, 134.6, 138.4, 138.4, 138.5, 139.3, 141.1, 145.9 ppm; IR (KBr): $\tilde{\nu} = 539, 722, 780, 798, 864, 875, 933, 1055, 1239, 1291, 1352, 1442, 2219$ (CN), 3091 cm⁻¹; and UV–Vis (dichloromethane, $c = 1 \times 10^{-5}$ mol dm⁻³): $\lambda_{\text{max}} = 234, 261, 364$ nm.

5-[5-(9H-Fluoren-9-ylidenemethyl)thiophen-2-yl]-1H-tetrazole (**4**, C₁₉H₁₂N₄S)

The mixture of 500 mg nitrile **3** (1.75 mmol), 340 mg NaN₃ (5.25 mmol), and 722 mg triethylamine hydrochloride (5.25 mmol) in 5.5 cm³ toluene was stirred at 100 °C for 18 h. Subsequently, reaction mixture was cooled down and extracted with water. To the aqueous layer, HCl (36%) was added dropwise to salt out the produced tetrazole. After filtration, the product was dried under reduced pressure and isolated in 92% yield (520 mg). Yellow powder; m.p.: 230 °C; ¹H NMR (300 MHz, DMSO-*d*₆): $\delta = 7.29$ (t, 1H, $J = 7.59$ Hz), 7.35 (t, 1H, $J = 7.47$ Hz), 7.39–7.43 (m, 2H), 7.68 (d, 1H, $J = 3.81$ Hz), 7.84 (d, 1H, $J = 7.5$ Hz), 7.88–7.94 (m, 2H), 7.94 (s, 1H), 7.98 (d, 1H, $J = 7.22$ Hz), 8.13 (d, 1H, $J = 7.85$ Hz) ppm; ¹³C NMR (75 MHz, DMSO-*d*₆): $\delta = 118.9, 119.9, 120.4, 121.0, 124.0, 126.8, 127.2, 127.3, 128.7, 129.4, 129.6, 131.6, 134.9, 136.6, 138.2, 138.8, 140.9, 141.8, 151.2$ ppm; and IR (KBr): $\tilde{\nu} = 721, 778, 873, 1049, 1145, 1445, 1454, 1597, 1620, 2740, 2784, 2862, 2913, 3052, 3087$ cm⁻¹.

Oxadiazoles synthesis

The solution of 200 mg tetrazole **4** (0.61 mmol), corresponding to aromatic 2-carbonyl chloride (0.86 mmol, 1.4 eq.) in 2 cm³ pyridine, was heated at 115 °C under argon atmosphere. The progress of the reaction was monitored by TLC. After 5 h, the reaction mixture was poured

into 70 cm³ water. The aqueous layer was filtered. The crude product was recrystallized and purified by column chromatography (hexane: EtOAc, 9:1).

2-[5-(9H-Fluoren-9-ylidenemethyl)thiophen-2-yl]-5-(thiophen-2-yl)-1,3,4-oxadiazole (**FLOX1c**, C₂₄H₁₄N₂OS₂)
Yield: 150 mg (60%); yellow powder; m.p.: 177–180 °C; ¹H NMR (300 MHz, CDCl₃): δ = 7.18–7.20 (m, 1H), 7.27–7.39 (m, 4H), 7.44 (dd, 1H, *J* = 3.9 Hz), 7.51 (s, 1H), 7.58 (dd, 1H, *J* = 5.1 Hz), 7.65–7.73 (m, 3H), 7.79–7.82 (m, 2H), 8.05 (d, 1H, *J* = 7.8 Hz) ppm; ¹³C NMR (75 MHz, CDCl₃): δ = 116.7, 119.4, 119.7, 120.2, 124.3, 124.4, 125.3, 126.8, 126.9, 128.0, 128.7, 129.2, 129.7, 129.9, 129.9, 130.2, 135.3, 138.4, 138.7, 138.9, 141.3, 143.7, 159.6, 160.1 ppm; and IR (KBr): $\tilde{\nu}$ = 706, 722, 775, 823, 855, 1024, 1035, 1062, 1353, 1444, 1485, 1574, 1617, 3074, 3104 cm⁻¹.

2-[5-(9H-Fluoren-9-ylidenemethyl)thiophen-2-yl]-5-phenyl-1,3,4-oxadiazole (**FLOX2a**, C₂₆H₁₆N₂OS)
Yield: 155 mg (63%); yellow powder; m.p.: 168–169 °C; ¹H NMR (300 MHz, CDCl₃): δ = 7.17–7.20 (m, 1H), 7.25 (s, 1H), 7.32–7.42 (m, 3H), 7.45–7.53 (m, 4H), 7.54–7.68 (m, 3H), 7.71 (s, 1H), 7.75 (d, 1H, *J* = 8.4 Hz), 7.87(d, 1H, *J* = 3.9 Hz), 8.07 (d, 1H, *J* = 7.8 Hz) ppm; ¹³C NMR (75 MHz, CDCl₃): δ = 116.9, 119.7, 119.9, 120.4, 123.5, 124.5, 126.9, 127.1, 127.2, 128.4, 128.8, 129.1, 129.2, 129.4, 130.1, 130.5, 131.8, 133.7, 134.5, 135.7, 139.2, 141.6, 144.1, 162.3, 171.9 ppm; and IR (KBr): $\tilde{\nu}$ = 686, 717, 729, 776, 857, 1025, 1066, 1274, 1352, 1447, 1486, 1547, 1582, 3051 cm⁻¹.

4-[5-[5-(9H-Fluoren-9-ylidenemethyl)thiophen-2-yl]-1,3,4-oxadiazol-2-yl]-*N,N*-dimethylaniline (**FLOX2c**, C₂₈H₂₁N₃OS)
Yield: 141 mg (52%); yellow powder; m.p.: 150–152 °C; ¹H NMR (300 MHz, CDCl₃): δ = 3.06 (s, 6H), 7.01 (s, 1H), 7.05–7.10 (m, 2H), 7.36–7.39 (m, 4H), 7.44 (dd, 1H, *J* = 3.9 Hz), 7.61–7.63 (m, 3H), 7.72–7.73 (m, 3H), 8.28 (d, 1H, *J* = 7.8 Hz) ppm; and ¹³C NMR (75 MHz, CDCl₃): δ = 41.3, 116.7, 119.4, 119.7, 121.0, 124.1, 124.4, 127.5, 128.4, 128.5, 128.7, 130.1, 136.8, 137.4, 137.5, 137.6, 140.2, 142.1, 155.3, 161.2, 164.5 ppm.

2-[5-(9H-Fluoren-9-ylidenemethyl)thiophen-2-yl]-5-(naphthalen-2-yl)-1,3,4-oxadiazole (**FLOX3c**, C₃₀H₁₈N₂OS)
Yield: 199 mg (72%); yellow powder; m.p.: 186–188 °C; ¹H NMR (300 MHz, CDCl₃): δ = 7.21 (t, 1H, *J* = 5.7 Hz), 7.31–7.42 (m, 3H), 7.50–7.51 (m, 1H), 7.57 (s, 1H), 7.61–7.65 (m, 2H), 7.70–7.77 (m, 3H), 7.93 (d, 1H, *J* = 3.0 Hz), 7.96 (d, 3H, *J* = 6.0 Hz), 8.05–8.09 (m, 2H), 8.28 (d, 1H, *J* = 5.5 Hz) ppm; ¹³C NMR (75 MHz, CDCl₃): δ = 116.9, 119.8, 120.0, 120.2, 120.5, 124.6, 124.9, 125.9, 126.2, 126.8, 127.1, 127.2, 128.2, 128.4, 128.7, 128.9, 129.4, 130.0, 130.2, 132.7, 133.8, 135.7,

137.3, 139.0, 139.1, 139.3, 141.6, 144.2, 160.1, 164.1 ppm; and IR (KBr): $\tilde{\nu}$ = 725, 740, 751, 768, 802, 823, 857, 1008, 1034, 1070, 1220, 1249, 1362, 1398, 1446, 1506, 1526, 1584, 3025 cm⁻¹.

2-[5-(9H-Fluoren-9-ylidenemethyl)thiophen-2-yl]-5-(3-methylbenzofuran-2-yl)-1,3,4-oxadiazole (**FLOX4c**, C₂₉H₁₈N₂O₂S)
Yield: 70%; yellow powder; m.p.: 228–230 °C; ¹H NMR (300 MHz, CDCl₃): δ = 2.72 (s, 3H), 7.18–7.23 (m, 1H), 7.30–7.42 (m, 4H), 7.44–7.50 (m, 2H), 7.55 (s, 1H), 7.60 (d, 1H, *J* = 6.9 Hz), 7.66–7.77 (m, 4H), 7.91 (d, 1H, *J* = 3.9 Hz), 8.05 (d, 1H, *J* = 7.8 Hz) ppm; ¹³C NMR (75 MHz, CDCl₃): δ = 9.6, 110.1, 111.5, 116.9, 119.2, 121.0, 123.3, 124.1, 124.6, 124.9, 127.5, 128.2, 128.4, 128.7, 128.9, 129.4, 130.1, 130.2, 136.8, 137.4, 137.5, 140.2, 142.1, 151.3, 154.1, 157.5, 161.2 ppm; and IR (KBr): $\tilde{\nu}$ = 718, 736, 769, 828, 875, 1029, 1074, 1138, 1266, 1342, 1358, 1380, 1404, 1442, 1454, 1485, 1578, 1616, 1634, 2922, 3073 cm⁻¹.

Optical spectroscopy and electrochemistry

The optical and electrochemical properties of synthesized **FLOXs** were determined by UV–Vis absorption and cyclic voltammetry measurements. The UV–VIS absorption spectra were taken on a UV 1650PC spectrometer (Shimadzu, Japan). Dichloromethane (CH₂Cl₂) was used for UV spectroscopy (Merck). The solution was measured in 1 cm cuvette. Fluorescence spectra were recorded on a Perkin–Elmer MPF-4 spectrofluorimeter (Norfolk, Connecticut USA). The cyclic voltammetry measurements were performed in solution, under nitrogen atmosphere with a computer-controlled electrochemical workstation (Amel 2053) in a three electrode single-compartment cells using platinum electrodes and SCE as the standard electrode, with ferrocene/ferricinium (Fc/Fc⁺) redox couple as internal standard, with a tetrabutylammonium tetrafluoroborate solution (0.1 M) in dichloromethane at a scan rate of 50 mV s⁻¹. The electric potential for ferrocene oxidation versus the standard hydrogen electrode *E*(Fc⁺/Fc) was 0.64 V.

Quantum chemical calculations

All quantum chemical calculations were done using the Gaussian 09 program package [24]. The optimal electronic ground-state geometries were found at the density functional level of theory employing Becke's three parameter hybrid functional using the Lee, Yang, and Parr correlation functions (B3LYP) [25, 26]. For the all-anti conformations, the initial setting of dihedral angle between thiophene and oxadiazole rings was +150°, and the dihedral angle

between oxadiazole and R group was -150° . Similar alternation of mutual aromatic plane orientations was used in the starting geometries of all-syn, syn-anti, and anti-syn conformations. The obtained structures were confirmed to be optimal by the standard normal mode analysis. On the basis of optimized B3LYP geometries, the vertical transition energies and oscillator strengths between the initial and final electronic states were computed by the time-dependent (TD)-DFT method [27]. These optical properties were calculated using the CAM-B3LYP (Coulomb-attenuating method applied to B3LYP) functional [28]. The 6-31+G(d,p) basis set was used [29, 30]. The energy cutoff used for all geometry optimizations was 4×10^{-3} - kJ mol^{-1} , and the final root mean square energy gradient was below $0.04 \text{ kJ mol}^{-1} \text{ \AA}^{-1}$. The influence of solvents was approximated by the continuum solvation model based on the quantum mechanical charge density, SMD [31] of a solute molecule interacting with a continuum description of the solvent. The visualization of the obtained theoretical results was done by the Molekel program package [32] and Gimp [33]. For the sake of comparison, we have evaluated the Boltzmann weighted quantities (Y) for dipole moments, vertical transition energies, and frontier orbital energies. The weighting overall conformers were performed according to Eq. (3):

$$Y = \sum_i w_i Y_i \quad (3)$$

where Y_i represents the calculated quantity for conformer i . The population of conformer i (w_i) with relative energy ΔE_i was calculated as

$$w_i = \frac{\exp(-\Delta E_i/kT)}{\sum_i \exp(-\Delta E_i/kT)} \quad (4)$$

where k is the Boltzmann constant, T is the thermodynamic temperature, and the relative energy ΔE_i was obtained with respect to the energy of the most stable conformer.

Acknowledgements This work has been supported by the Slovak Grant agency VEGA 1/0594/16, 1/0829/14, 1/0601/15, 2/0142/14 and APVV-0038-11, APVV-15-0079, and NANOSILK CNR-SAS Joint Research Project. The authors also thank Marcela Kimličková (SAS-PI) for the UV analysis. We are grateful to the HPC center at the Slovak University of Technology in Bratislava, which is a part of the Slovak Infrastructure of High-Performance Computing (SIVVP Project, ITMS code 26230120002, funded by the European Region Development Funds, ERDF) for the computational time and resources made available.

References

- Sun Y, Welch GC, Leong WL, Takacs CJ, Bazan GC, Heeger AJ (2012) *Nat Mater* 11:44
- Martínez-Díaz MV, Ince M, Torres T (2011) *Monatsh Chem* 142:699
- Kozma E, Catellani M (2013) *Dyes Pigm* 98:160
- Fernandez-Hernandes JM, Beltran JI, Lemaur V, Galvez-Lopez MD, Chien CH, Polo F, Orselli E, Fröhlich R, Cornil J, De Cola L (2013) *Inorg Chem* 52:1812
- Miao S, Zhu Y, Bao Q, Li H, Li N, Ji S, Xu Q, Lu J, Wang LJ (2014) *Phys Chem C* 118:2154
- Müllen K, Wegner G (1998) *Electronic Materials: The Oligomer Approach*. Wiley, Weinheim
- Lukeš V, Matis M, Végh D, Štefko M, Hrdlovič P, Laurinc V (2007) *Synth Met* 157:770
- Danko M, Andicsová A, Hrdlovič P, Racko D, Végh D (2013) *Photochem Photobiol Sci* 12:1210
- Usluer O, Demic S, Egbe DAM, Bircikner E, Tozlu C, Pivrikas A, Montaigne Ramil A, Sariciftci NS (2010) *Adv Funct Mater* 20:4152
- Dumur F, Goubard F (2014) *New J Chem* 38:2204
- Murali MG, Naveen P, Udayakumar D, Yadav V, Srivastava R (2012) *Tetrahedron Lett* 53:157
- Zhu Y, Fan X, Jiang X, Zhang Y, Chen Z (2015) *Org Biomol Chem* 13:10402
- Savarino A (2006) *Expert Opin Investig Drugs* 15:1507
- James ND, Growcott JW (2009) *Drugs Future* 34:624
- Polshettiwar V, Varma RS (2008) *Tetrahedron Lett* 49:879
- Sitha S, Bhanuprakash K (2006) *J Mol Struct (Theochem)* 761:31
- Puschnig P, Ambrosch-Draxl C (2008) *Monatsh Chem* 139:389
- Zhao B, Liu D, Peng L, Li H, Shen P, Xiang N, Tan S (2009) *Eur Polym J* 45:2079
- Bouzzine SM, Bouzakraoui S, Bouachrine M, Hamidi M (2005) *J Mol Struct (Theochem)* 726:271
- Hammitt LP (1937) *J Am Chem Soc* 59:96
- Blouin N, Michaud A, Gendron D, Wakim S, Blair E, Neagu-Plesu R, Leclerc M (2008) *J Am Chem Soc* 130:732
- Bredas JL, Silbey R, Boudreaux DS, Chance RR (1983) *J Am Chem Soc* 105:6555
- Perašinová L, Štefko M, Végh D, Kožíšek J (2006) *Acta Crystallogr Sect E: Struct Rep Online* 62:o3972
- Frisch MJ, Trucks GW, Schlegel HB, Scuseria GE, Robb MA, Cheeseman JR, Scalmani G, Barone V, Mennucci B, Petersson GA, Nakatsuji H, Caricato M, Li X, Hratchian HP, Izmaylov AF, Bloino J, Zheng G, Sonnenberg JL, Hada M, Ehara M, Toyota K, Fukuda R, Hasegawa J, Ishida M, Nakajima T, Honda Y, Kitao O, Nakai H, Vreven T, Montgomery JA Jr, Peralta JE, Ogliaro F, Bearpark M, Heyd JJ, Brothers E, Kudin KN, Staroverov VN, Kobayashi R, Normand J, Raghavachari K, Rendell A, Burant JC, Iyengar SS, Tomasi J, Cossi M, Rega N, Millam JM, Klene M, Knox JE, Cross JB, Bakken V, Adamo C, Jaramillo J, Gomperts R, Stratmann RE, Yazyev O, Austin AJ, Cammi R, Pomelli C, Ochterski JW, Martin RL, Morokuma K, Zakrzewski VG, Voth GA, Salvador P, Dannenberg JJ, Dapprich S, Daniels AD, Farkas Ö, Foresman JB, Ortiz JV, Cioslowski J, Fox DJ (2009) *Gaussian 09, Revision D.01*. Gaussian, Inc, Wallingford
- Lee C, Yang W, Parr RG (1988) *Phys Rev B* 37:785
- Becke AD (1993) *J Chem Phys* 98:5648
- Furche F, Ahlrichs R (2002) *J Chem Phys* 117:7433
- Yanai T, Tew DP, Handy NC (2004) *Chem Phys Lett* 393:51
- Hehre WJ, Ditchfield R, Pople JA (1972) *J Chem Phys* 56:2257
- Rassolov V, Ratner M, Pople J, Redfern P, Curtiss LJ (2001) *Comput Chem* 22:996
- Marenich AV, Cramer CJ, Truhlar DG (2009) *J Phys Chem B* 113:6378
- Varetto U (2009) Molekel 5.4.0.8. Swiss National Supercomputing Centre, Lugano
- The GIMP Team (2016) GIMP 2.8.18. <http://www.gimp.org>. Accessed 20 May 2016